Title

The structure of an iron-containing alcohol dehydrogenase from a hyperthermophilic archaeon in two chemical states.

Journal

Acta Crystallographica Section F: Structural Biology Communications, 75(Pt 4)

Authors

Larson, Steven
Jones, Jesse
Mcpherson, Alexander

Publication Date

2019-04-01

DOI

10.1107/S2053230X19001201

Peer reviewed

STRUCTURAL BIOLOGY COMMUNICATIONS

ISSN 2053-230X

The structure of an iron-containing alcohol dehydrogenase from a hyperthermophilic archaeon in two chemical states

Steven B. Larson,[a] Jesse A. Jones[b] and Alexander McPherson[a]*

[a]Department of Molecular Biology and Biochemistry, University of California, 530A Steinhaus Hall, Irvine, CA 92697-3900, USA, and [b]Department of Pharmaceutical Sciences, University of Tennessee Health Science Center, 881 Madison Avenue, Memphis, TN 38163, USA. *Correspondence e-mail: amcphers@uci.edu

Received 30 October 2018
Accepted 22 January 2019

Edited by N. Sträter, University of Leipzig, Germany

Keywords: NADP; oxidation–reduction; thermophile; active site; dimers; alcohol dehydrogenase; *Thermococcus thioreducens*.

PDB references: iron-containing alcohol dehydrogenase, tetragonal form, 6c7l; monoclinic form, 6c75; orthorhombic form, 6c76

Supporting information: this article has supporting information at journals.iucr.org/f

An iron-containing alcohol dehydrogenase (FeADH) from the hyperthermophilic archaeon *Thermococcus thioreducens* was crystallized in unit cells belonging to space groups $P2_1$, $P2_12_12_1$ and $P4_32_12$, and the crystal structures were solved at 2.4, 2.1 and 1.9 Å resolution, respectively, by molecular replacement using the FeADH from *Thermotoga maritima* (Schwarzenbacher *et al.*, 2004) as a model. In the monoclinic and orthorhombic crystals the dehydrogenase (molecular mass 41.5 kDa) existed as a dimer containing a twofold noncrystallographic symmetry axis, which was crystallographic in the tetragonal crystals. In the monoclinic and orthorhombic asymmetric units one molecule contained iron and an NADP molecule, while the other did not. The tetragonal crystals lacked both iron and NADP. The structure is very similar to that of the FeADH from *T. maritima* (average r.m.s. difference for C^{α} atoms of 1.8 Å for 341 aligned atoms). The iron, which is internally sequestered, is bound entirely by amino acids from one domain: three histidines and one aspartic acid. The coenzyme is in an extended conformation, a feature that is common to the large superfamily of NADH-dependent dehydrogenases that share a classical nucleotide-binding domain. A long broad tunnel passes entirely through the enzyme between the two domains, completely encapsulating the coenzyme.

1. Introduction

Alcohol dehydrogenases (ADHs) are ubiquitous enzymes that catalyze the oxidation of alcohols and the reduction of aldehydes for a large variety of physiological purposes (Brändén & Tooze, 1999; Eklund & Brändén, 1987; Persson *et al.*, 2008; Petsko & Ringe, 2004; Walsh, 1979). These range from eliminating ethanol in higher organisms to providing reducing power for the production of essential metabolic intermediates. They are present in all living organisms, including human beings and archaea at the two ends of the evolutionary spectrum. The substrate specificity of alcohol dehydrogenases can be broad to include alkyl, aromatic and branched alcohols, or narrow to accept only primary alkyl alcohols. For many of the alcohol dehydrogenases the affinity for aldehydes is significantly greater than that for alcohols. The enzymes frequently have very specific responsibilities or narrow substrate requirements in complex catabolic or anabolic pathways.

Several categories of ADH can be distinguished based on cofactor or coenzyme specificity (Radianingtyas & Wright, 2003), these being (i) NAD or NADP, (ii) the pyrroloquinoline quinine, haem or cofactor F_{420} and (iii) FAD. The NAD(P)-dependent ADHs can further be subdivided into (i) zinc-dependent ADHs, (ii) short-chain ADHs and (iii) iron-containing and iron-activated ADHs. ADHs are classified as iron-containing if they contain an essential Fe atom in their

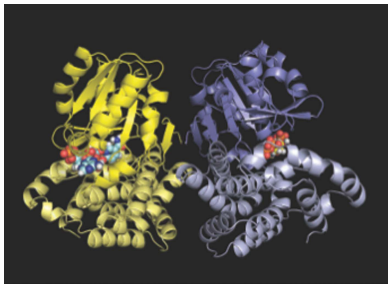

structure at the end of their purification, while iron-activated enzymes may be vacant after purification but require iron in the assay mixture in order for activity to be observed (Liu *et al.*, 2009).

ADHs in virtually all higher organisms are of the zinc-containing variety, and such organisms often possess only a single type, although isozymes from several genes may be expressed. Their function is generally to eliminate ethanol. In microorganisms, including thermophilic bacteria, the array of ADHs that are expressed may be considerably more diverse, and as many as half a dozen different types of ADH can be detected in extracts or by analysis of the genome, most of which are also zinc enzymes. Among the ADHs, however, iron-containing ADHs (FeADHs) are also common. There is one example, from *Pyrococcus furiosus*, of an ADH that contains both iron and zinc (Ma & Adams, 1999). Rare examples also exist of ADH enzymes that contain metal ions other than iron or zinc (Elleuche & Antranikian, 2013). All ADHs from thermophilic bacteria, with a lone exception, use NADP and NADPH as cofactors in the redox reaction (Radianingtyas & Wright, 2003). The functional roles and the substrates on which the enzymes act are often unknown or ambiguous in these bacteria, as are the extents of their substrate specificity. ADHs from thermophilic archaea and bacteria, and their roles, properties and phylogeny, have been ably reviewed by Radianingtyas & Wright (2003).

Here, we describe the structure solution by X-ray diffraction, using molecular-replacement techniques, of three different crystallographic unit cells of an iron-containing ADH from the hyperthermophilic archaeon *Thermococcus thioreducens* (Pikuta *et al.*, 2007), designated strain OGL-20P and collected from a hydrothermal black smoker in the Rainbow Vent Site in the Atlantic Ocean in 2007. The bacteria grow between 55 and 94°C, with an optimum of 83–85°C at pH 7. The microorganism is a heterotrophic strict anaerobe, which is obligately dependent on elemental sulfur and is catalase-negative. Phylogenetic analysis based on 16S RNA sequences indicates strain OGL-20P to be a new species within the *Thermococcus* genus in the Archaea (Pikuta *et al.*, 2007).

The entire genome has been analyzed and many of the 2301 sequences that could potentially code for proteins have been cloned into *Escherichia coli* and expressed (iXpressGenes, Huntsville, Alabama, USA). Among these is a protein that has been identified as an iron-containing ADH. Assignment of function was based on amino-acid sequence (UniProt identifier A0A0Q2QQL1) homology to the iron-containing ADH from *Thermotoga maritima* (UniProt identifier Q9X022). The *T. thioreducens* FeADH gene codes for a polypeptide composed of 378 amino acids that has a molecular mass of 41.5 kDa. The FeADH from *T. thioreducens* has 23.70% sequence identity, with 91 identical and 141 homologous amino acids, to the FeADH enzyme from *T. maritima* based on a *FASTA* alignment (*Clustal Omega*).

The enzyme from *T. maritima*, which is similar to the FeADH studied here, is thought to possess catalytic activity with short-chain primary alcohols such as 1,3-propanediol, but beyond this its specificity is obscure at best. The same can be said for the enzyme from *T. thioreducens*. The nature of the Fe atom bound by the ADH is also ambiguous, and may be a mixture of iron in the ferrous and ferric states (Radianingtyas & Wright, 2003). Whether this has an effect on its binding by the protein, its interaction with the coenzyme or its regulatory role is not known.

To our knowledge, the only thermophilic iron-containing ADH for which a structure has been determined by X-ray diffraction is the enzyme from *T. maritima* (Schwarzenbacher *et al.*, 2004). A recombinant form of this protein was solved at cryogenic temperature using MAD phasing based on selenomethionine anomalous scattering, and was refined to 1.3 Å resolution (Schwarzenbacher *et al.*, 2004). Iron-containing ADHs from nonthermophilic bacteria, however, have also been analyzed by X-ray crystallography (Montella *et al.*, 2005; Moon *et al.*, 2011). We have grown three different crystal forms of the enzyme from *T. thioreducens* and, using the model of the protein from *T. maritima* (Schwarzenbacher *et al.*, 2004) as a probe, solved the structures of the three crystal forms.

2. Experimental

2.1. Cloning

The coding sequence for the iron-containing alcohol dehydrogenase (FeADH) was PCR-amplified against the genomic DNA of *T. thioreducens* and was inserted into the pET-3a expression vector (Novagen, Madison, USA). The PCR oligonucleotide primers were designed to include additional 3′ and 5′ vector-specific sequences to facilitate ligation-independent cloning. The forward primer sequence consisted of 30 nt of the pET-3a vector sequence upstream of the NdeI site, followed by a 20 nt sequence corresponding to the N-terminal sequence of FeADH. Similarly, the reverse primer consisted of 32 nt of the pET-3a vector sequence downstream of the BamHI site and a 22 nt sequence corresponding to the C-terminal sequence of FeADH. The oligonucleotides were synthesized by Operon (Huntsville, Alabama, USA) and were diluted to a working concentration of 2 µ*M*. The primer sequences are shown in Table 1.

PCR amplification was performed in a PerkinElmer GeneAmp PCR System 9600 thermal cycler. The DNA mixture was initially heated for 5 min, followed by 25 cycles of denaturation at 95°C for 30 s, annealing at 55°C for 30 s and extension at 72°C for 30 s. The reaction was terminated by 5 min of extension at 72°C. The amplification reaction took place in a 100 µl volume and included *PfuUltra* II Fusion HS DNA Polymerase (Stratagene, La Jolla, California, USA) and its corresponding buffer according to the manufacturer's instructions, dNTPs at a final concentration of 2 m*M* each, 50 m*M* of each oligonucleotide and 10 ng of genomic DNA.

Linearized pET-3a vector was prepared using 5 µg of the plasmid, which was double-digested with the NdeI and BamHI restriction endonucleases (Promega, Madison, Wisconsin, USA) following the manufacturer's instructions. The digested plasmid was purified using the QIAquick PCR Purification Kit

(Qiagen, Valencia, California, USA) and blunt-ended with the Klenow fragment (Promega, Madison, Wisconsin, USA), according to the manufacturer's directions. The resulting pET-3a fragment was used for homologous recombination reactions without further modification. Approximately 40 ng of the resulting amplified product was mixed with an equal amount of the linearized expression vector, and the resulting mixture was transformed into chemically competent DH5 *E. coli* cells as described by Marsic *et al.* (2008). This method of cloning was possible because the 5′ and 3′ extreme DNA ends flanking the FeADH open reading frame were designed to be homologous to the end sequences of a prepared linear expression vector. When the DNA fragment was mixed with the prepared linear expression vector and transformed into competent *E. coli* cells (for example DH5), an intrinsic recombinase activity joined the two DNA fragments. This resulted in a circular expression plasmid containing the coding region of the targeted protein. Thus, cloning can be performed without the use of overnight ligation or restriction enzymes. To accomplish this, 40 ng of the prepared linear vector was mixed with 100 ng of the amplified DNA sequence in a sterile microcentrifuge tube on ice. After 20 min, the mixture was used for transformation into DH5 competent *E. coli* cells. This was accomplished by adding the entire mixture (∼5 µl) to 50 µl of competent cells thawed on ice. After 30 min of incubation, the cells were heat-shocked at 42°C for 1 min. Thereafter, the transformed cells were diluted with 400 µl Luria–Bertani (LB) medium and incubated for 1 h at 37°C before being spread on LB–agar plates containing 100 mg l^{-1} carbenicillin. Colonies were grown overnight in selective LB Miller broth to propagate the recombinant plasmid. The plasmids were then extracted by standard molecular biology protocols (Sambrook *et al.*, 1989) using a Qiagen Plasmid Miniprep Kit according to the manufacturer's instructions. Finally, the purified plasmids were sequenced by the MWG DNA-sequencing service to identify the clones that contained the correct (Novagen, Madison, USA) coding sequence.

2.2. Transformation

The sequence-confirmed plasmid construct was transformed into *E. coli* Rosetta2 cells (Novagen) for expression by adding approximately 20 ng plasmid DNA to 50 µl of competent cells. After 30 min of incubation on ice, the cells were heat-shocked at 42°C for 1 min. The transformed cells were then diluted with 400 µl LB medium and incubated for 1 h at 37°C before being spread onto LB–agar plates containing 100 mg l^{-1} carbenicillin and 35 mg l^{-1} chloramphenicol.

2.3. Glycerol stocks

Glycerol stocks were stored from first-generation growth cultures that had been inoculated with a single colony of the transformed expression host. The cells were taken from the growth culture during the exponential growth phase just prior to IPTG induction. Sterile glycerol was added to 1 ml aliquots of the cell suspension to reach a final concentration of 12%. Gentle agitations of the sample mixtures were performed to allow the glycerol to evenly distribute within the cell suspension. The solutions were prepared in sterilized 1.5 ml microcentrifuge tubes and stored at −80°C. These stocks were used as starter inoculates for overnight cultures for all subsequent large-scale protein-expression experiments.

Table 1
Protein cloning and expression.

Source organism	*T. thioreducens*
Forward primer	5′-TTTGTTTAACTTTAAGAAGGAGATATACATA TGTTCTGGCTGAAAACCCG-3′
Reverse primer	5′-CTTCCTTTCGGGCTTTGTTAGCAGCCGGATC CTCATTCTCCCCTGTATGCCTTG-3′
Expression vector	pET-3a (Novagen) containing NdeI/BamHI insertion sites
Genome accession code	CP015105
Host	*E. coli* DH5 cells
Amino-acid sequence	MFWLKTRIIEGEGSLSRLSREVKGHERVLILASG SMKRHGFLSEAEDYVKEAGAEVFSIAGLPAEP SVEVIEEFLPKVREFGPDLLVAMGGGSVIDTT KALKVFYDAPELNFGEIAFIDRFSKPKPVPRL KTLLIAIPSTSGAGSEVSGASVLKKGGVKYNI VTPEIAPDVAILDPRLPRTMPPEVARNSGLDV LVHGIEAYTTKVASPFSDAMAIKAIKTVYRWL PLSVKGDEEARARVHYAATMAGIAFLNARLGL CHAMSHKAAWIGPHGLLNAVFLPYVMEFNASK SDYARRRYAEIARELGFQTAKDLIEVVKELNE MLGVPKLGELVDEETFASKVEEMAEKTYHDGL IAFNPVEPKPEEIKELYLKAYRGE
NCBI protein ID	ASJ12775

2.4. Expression of FeADH

Cultures for recombinant expression were grown in 2 l LB broth containing 100 g ml^{-1} carbenicillin and 35 g ml^{-1} chloramphenicol. Following inoculation of the 2 l culture with a 10 ml overnight starter culture, the cells were allowed to propagate at 37°C until the point of induction, corresponding to an optical density ($OD_{600\ nm}$) of 0.8. At this point, protein expression was induced by the addition of isopropyl β-D-1-thiogalactopyranoside (IPTG) to a final concentration of 1 m*M*, and the culture was then transferred to a refrigerated incubator and shaken overnight at 250 rev min^{-1} at 18°C. After 18 h, the cells were harvested by centrifugation at 8000*g* using a JLA 9.1000 rotor in a Beckman Avanti J-25 centrifuge.

2.5. Purification

Purification of FeADH was accomplished by resuspending the pellet (∼10 g wet weight) in 100 ml buffer *A* (50 m*M* Tris pH 7.5, 50 m*M* NaCl, 1 m*M* EDTA). The cells were disrupted by eight cycles of sonication using a Branson Sonifier 250 cell disruptor (VWR Scientific, USA). The resulting lysate was centrifuged for 20 min at 10 000*g* using a JA-25.50 rotor, and the supernatant was subjected to heat treatment for 30 min in an Erlenmeyer flask submersed in a 75°C water bath. The denatured protein was removed by centrifugation at 10 000*g* for 20 min with the same rotor, and the supernatant was loaded onto a 5 ml HiTrap Q Sepharose XL cation-exchange column (GE Heathcare, USA) that had been pre-equilibrated with buffer. The loading buffer used for anion exchange consisted of 0.05 *M* Tris pH 7.5, 0.05 *M* NaCl, 1 m*M* EDTA

Table 2
Crystallization.

Crystal form	Monoclinic	Orthorhombic	Tetragonal
Method	Vapor diffusion	Vapor diffusion	Vapor diffusion
Plate	Cryschem	Cryschem	Cryschem
Temperature (K)	293	293	293
Protein concentration (mg ml^{-1})	20	20	20
Protein buffer	Water	Water	Water
Reservoir solution	8% PEG 4000 pH 4.5	8% PEG 4000 pH 4.5	0.4 *M* $NH_4H_2PO_4$ pH 4.2
Protein:reservoir ratio	2:1	2:1	1:1
Reservoir volume (ml)	0.6	0.6	0.6
Cryoprotectant	None	None	20% PEG 3350 + 30% MPD in reservoir solution

Table 3
Data collection and processing.

Values in parentheses are for the outer shell.

Crystal form	Monoclinic	Orthorhombic	Tetragonal
Diffraction source	Rigaku MicroMax-007 HF	Rigaku MicroMax-007 HF	Rigaku MicroMax-007 HF
Wavelength (Å)	1.54187	1.54187	1.54187
Temperature (K)	298	298	100
Detector	Saturn 944+	Saturn 944+	Saturn 944+
Crystal-to-detector distance (mm)	80	80	100
Rotation range per image (°)	0.5	0.5	0.5
Total rotation range (°)	148, 148, 50, 50	150, 150, 150, 90, 157.5, 150, 90, 150	90.5
Exposure time per image (s)	18	15	10 (3 scans), 30 (2 scans)
No. of crystals	2	5	1
Space group	$P2_1$	$P2_12_12_1$	$P4_32_12$
a, *b*, *c* (Å)	59.13, 99.25, 67.49	48.92, 111.98, 142.08	69.30, 69.30, 166.64
α, β, γ (°)	90, 103.16, 90	90, 90, 90	90, 90, 90
Average mosaicity (°)	0.74	0.56	0.68
Resolution range (Å)	49.61–2.40 (2.49–2.40)	43.97–2.10 (2.16–2.10)	29.00–1.909 (1.93–1.909)
Total No. of reflections	151331 (1175)	853540 (3198)	639242 (5238)
No. of unique reflections	23385 (677)	41831 (1309)	30956 (1343)
Completeness (%)	79.0 (22.0)	90.0 (35.6)	95.2 (84.6)
Multiplicity	6.5 (1.7)	20.4 (2.4)	20.7 (3.9)
$\langle I/\sigma(I)\rangle$	12.0 (1.8)	13.0 (0.7)	12.5 (1.6)
R_{merge}	0.234 (0.749)	0.209 (0.974)	0.096 (0.673)
R_{meas} ($R_{r.i.m.}$)	0.253 (0.993)	0.214 (1.192)	0.098 (0.768)
$R_{p.i.m.}$	0.092 (0.646)	0.041 (0.670)	0.020 (0.355)
Overall *B* factor from Wilson plot (Å^2)	48.6	36.7	28.8
$CC_{1/2}$	0.982 (0.368)	0.995 (0.222)	0.999 (0.647)

and the elution buffer was 0.05 *M* Tris pH 7.5, 1 *M* NaCl, 1 m*M* EDTA. The protein was eluted at a flow rate of 2.5 ml min^{-1} into 2.5 ml fractions with a gradient from 0.05 to 1.0 *M* NaCl using an ÄKTAexplorer FPLC system (Amersham Pharmacia). The collected fractions corresponding to the major elution peak were pooled and concentrated to a volume of 2 ml using a Centricon-10 ultrafiltration device (Millipore) and loaded onto a Sephadex S-200 size-exclusion column. The column was pre-equilibrated with an elution buffer consisting of 50 m*M* Tris pH 7.5, 50 m*M* NaCl buffer. No EDTA was added to the final elution buffer. The fractions of the principal elution peak from the size-exclusion column were eluted using approximately 60 ml buffer and were collected and analyzed by SDS–PAGE.

2.6. Crystallization

The crystallization of all crystal forms is summarized in Table 2, although some details are worth reprising here. Two crystal forms of the FeADH from *T. thioreducens* were grown under very similar conditions, and occasionally both forms were observed in the same sample of mother liquor. These were monoclinic (space group $P2_1$) and orthorhombic (space group $P2_12_12_1$) forms (see Table 3) and were obtained by vapor diffusion (McPherson, 1999; McPherson & Gavira, 2014) in Cryschem sitting-drop plates (Hampton Research, Aliso Viejo, California, USA). The drops initially consisted of 2 µl reservoir solution plus 2 µl water plus 4 µl 20 mg ml^{-1} protein in water. The 0.6 ml reservoir for the monoclinic crystals consisted of 0.1 *M* sodium acetate pH 4.5, 8% PEG 4000. For the orthorhombic crystals, the reservoir consisted of 0.1 *M* sodium acetate pH 4.6, 10% PEG 10 000. When the drops were formulated in the sitting-drop plates, some precipitate began forming immediately. The drops were clarified by addition of 2 µl 1 *M* ammonium hydroxide to achieve a more alkaline pH. As volatile ammonia was lost to the reservoir by vapor diffusion, the pH of the drops returned to a weakly acid level and the crystals nucleated and grew. The occasional single-drop polymorphism suggests that the PEG molecular weight and concentration were of minor importance.

The third crystal form (space group $P4_32_12$) had a tetragonal bipyramid habit and was obtained under quite different

Table 4
Structure solution and refinement.

Values in parentheses are for the outer shell.

Crystal form	Monoclinic	Orthorhombic	Tetragonal
PDB entry/model used in molecular replacement	1o2d	Monoclinic form	Orthorhombic form
Resolution range (Å)	49.6–2.4 (2.5–2.4)	33.0–2.1 (2.2–2.1)	29.00–1.91 (2.00–1.91)
Completeness (%)	78.88 (19.35)	89.82 (32.73)	94.83 (80.76)
σ Cutoff	None	None	None
No. of reflections used	22218	39750	28792
No. of reflections, working set	21068 (402)	37732 (1057)	26795 (1997)
No. of reflections, test set	1150 (21)	2018 (55)	1774 (127)
Final R_{cryst}	0.14 (0.30)	0.15 (0.35)	0.13 (0.29)
Final R_{free}	0.21 (0.35)	0.20 (0.39)	0.19 (0.35)
Cruickshank DPI	0.20	0.23	0.14
No. of non-H atoms			
Protein	5852	5994	3165
Ions†	1	1	95
Coenzymes‡	79	48	31
Other ligands§	—	14	12
Water	167	293	462
Total	6099	6350	3765
R.m.s. deviations			
Bonds (Å)	0.003	0.005	0.008
Angles (°)	0.61	0.96	1.12
Average B factors (Å^2)			
Protein	66	45	41
Ions†	70	65	61
Coenzymes‡	80	41	72
Other ligands§	—	73	100
Water	57	49	52
All atoms	66	46	43
Ramachandran plot			
Favored regions (%)	97.2	96.4	97.9
Additionally allowed (%)	2.8	3.5	2.1
Outliers (%)	0.0	0.1	0.0
PDB code	6c75	6c76	6c7l

† Ions are Fe^{3+} in molecules *A* of PDB entries 6c75 and 6c76 and PO_4^{3-} in PDB entry 6c7l. ‡ Coenzymes are NADP (NAP) and 2′-monophosphoadenosine 5′-diphosphate (ATR). NADP is present in molecules *A* of PDB entries 6c75 and 6c76, and ATR is present in PDB entry 6c7l and molecule *B* of PDB entry 6c75. § Other ligands are acetic acid (ACY) and triethylene glycol (PGE) in PDB entry 6c76 and 1,2-ethanediol (EDO) and MPD in PDB entry 6c7l.

conditions. Vapor diffusion was again used as above, but the droplet was composed of equal amounts of the stock protein solution and a reservoir consisting of 0.4 *M* $NH_4H_2PO_4$ pH 4.2. All crystallization was carried out at room temperature. The V_M and percentage solvent for the crystals were monoclinic, $V_M = 2.32$ Å^3 Da^{-1}, 47% solvent content; orthorhombic, $V_M = 2.34$ Å^3 Da^{-1}, 47% solvent content; tetragonal, $V_M = 2.41$ Å^3 Da^{-1}, 49% solvent content. These are all relatively low values (McPherson, 1999) and indicate close packing of the molecules in all crystal forms.

2.7. Data collection

Monoclinic and orthorhombic crystals were mounted in 0.8 mm quartz capillaries by conventional means (McPherson, 1982) and X-ray diffraction data were recorded at room temperature using a Rigaku MicroMax-007 HF generator operated at 40 kV and 30 mA and a Saturn 944+ CCD detector. Data-collection parameters can be found in Table 3. Crystal decay was not significant and generally at least two orientations in χ were collected. Images were processed with *iMosflm* (Battye *et al.*, 2011). Structure amplitudes were obtained by scaling and merging intensities using *AIMLESS* (Blessing, 1997; Evans, 2006, 2011; Evans & Murshudov, 2013) to yield highly redundant data sets (Table 3). Crystals of the tetragonal modification were immersed in a cryoprotective solution composed of 0.4 *M* $NH_4H_2PO_4$, 20% PEG 3350, 30% MPD for 15 s and were then flash-cooled in liquid nitrogen. The data were collected using similar instruments at cryogenic temperature (Pflugrath, 2004, 2015) and were integrated, scaled and merged with *HKL*-3000 (Minor *et al.*, 2006). The resolutions of the diffraction data used in refinement were 2.4 Å for the $P2_1$ crystals, 2.1 Å for the $P2_12_12_1$ crystals and 1.9 Å for the $P4_32_12$ crystals.

2.8. Structure solution and refinement

The structure of the enzyme in the monoclinic crystals was solved in a straightforward manner by molecular replacement using *Phaser* (McCoy *et al.*, 2007). The model of FeADH from *T. maritima* (PDB entry 1o2d) was used as a probe. Sequence replacement, rebuilding and most graphics operations relied on *Coot* (Emsley *et al.*, 2010). The monoclinic crystal structure was then used in *Phaser* to solve the structure of the orthorhombic form, and a preliminary orthorhombic model was used to solve the structure of the tetragonal crystal form using *Phaser*. Refinements of the models of the protein and associated small molecules in all three crystal forms were carried

out using *REFMAC* (Murshudov *et al.*, 2011) from the *CCP*4 program suite, based on a maximum-likelihood approach (Murshudov *et al.*, 1997). Illustrations were prepared using *PyMOL* (Schrödinger).

3. Results

Table 4 contains refinement and model statistics, including the identification of the model components for each structure. The monoclinic and orthorhombic crystal forms, both grown using PEG, have two molecules of the enzyme in the asymmetric unit. In both cases the two molecules are not the same but represent different chemical states of the protein. In each structure molecule *A* contains an Fe atom and the dinucleotide coenzyme NADP. The other molecule, molecule *B*, does not. In the monoclinic crystal the coenzyme site of chain *B* is approximately 75% occupied by 2′-monophosphoadenosine 5′-diphosphate (ATR), lacking both the Fe atom and the nicotinamide-ribosyl moiety; the NADP-binding site in chain *B* of the orthorhombic crystal is essentially devoid of any coenzyme, although contouring the $2F_o - F_c$ map down to about 0.15σ reveals density consistent with a very minor NADP or ATR component similar to that found in the monoclinic crystal (see Fig. 1 and Supplementary Figs. S1 and S2). This arrangement in the asymmetric unit differed from that found for the enzyme from *T. maritima*, in which both molecules in the asymmetric unit of the crystal contained an Fe atom and an NADP molecule.

The tetragonal form of the enzyme, grown from ammonium dihydrogen phosphate, is most different in that it has only a single protein molecule in the asymmetric unit. This molecule lacks both NADP and an Fe atom but, similar to molecule *B* of the monoclinic form, the NADP-binding site contains ATR, which was modeled at 60% occupancy (see Supplementary Fig. S3). The conformation of the protein in the tetragonal crystals is, within the error limits of the structure determination, the same (the average r.m.s.d. is 0.62 Å over 378 C^{α} atoms) as in the *B* molecules of the other two crystal forms (see Supplementary Table S1*a*).

The structural results suggest that FeADH from *T. thioreducens* is a dimer under both high-salt and low-salt conditions. Two identical subunits are related by a nearly exact NCS twofold axis in both the monoclinic and orthorhombic crystals. The monoclinic and orthorhombic dimeric asymmetric units superimpose exactly (r.m.s.d. of 0.42 Å; Supplementary Table S1*b*), and the two molecules share a large, intimate interface, as seen in Fig. 1(*c*). In the tetragonal crystals, pairs of molecules are related by crystallographic twofold axes. If two molecules related by an exact, crystallographic dyad in the tetragonal crystals are taken as a dimer, this dimer superimposes well on the asymmetric units of both the monoclinic and the orthorhombic crystals (average r.m.s.d. of 1.09 Å;

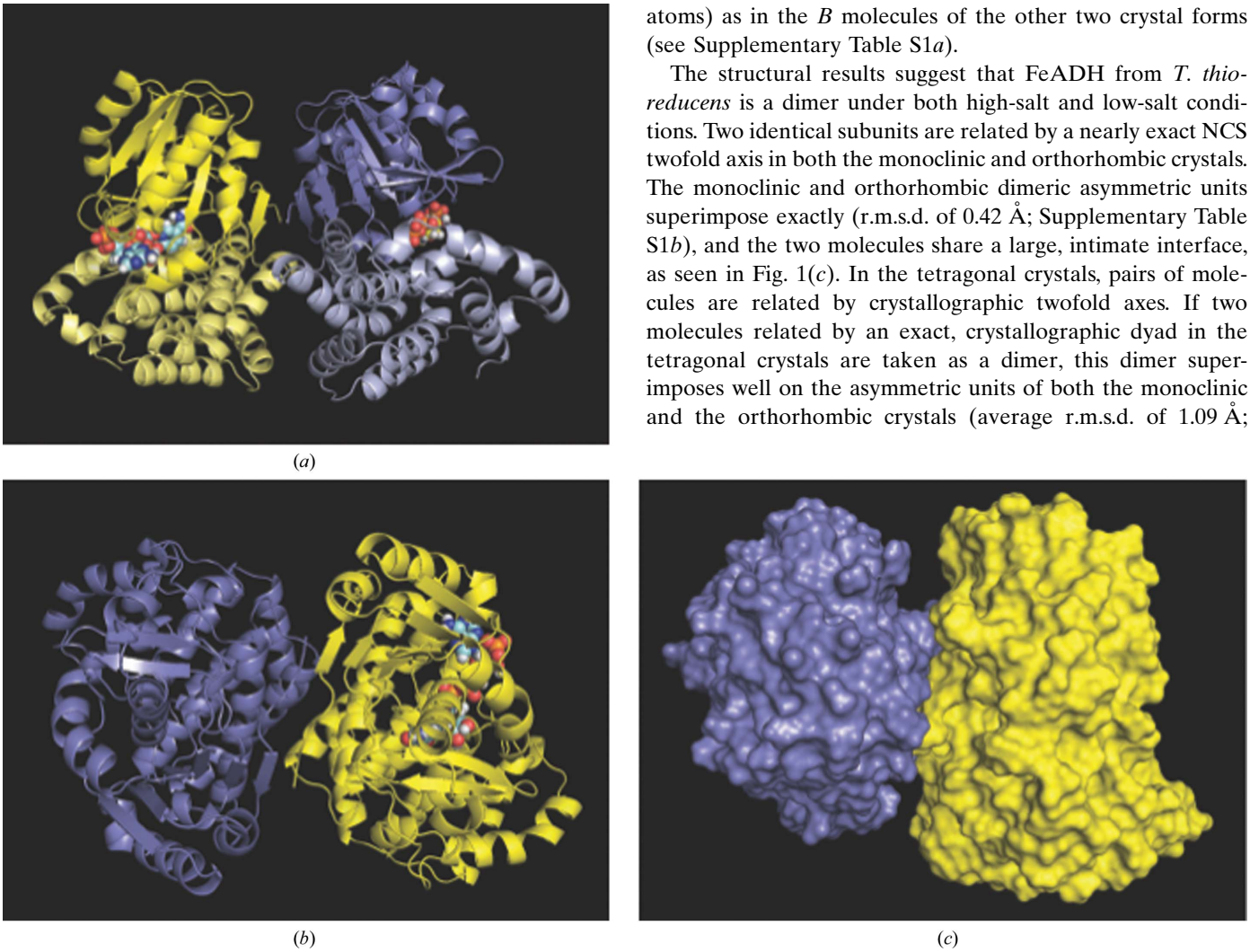

(*a*) (*b*) (*c*)

Figure 1
Molecular structures. (*a*) The two FeADH molecules in the monoclinic cell composing the dimeric asymmetric unit shown in schematic format viewed perpendicular to the NCS twofold axis. (*b*) The FeADH dimer from the orthorhombic cell viewed down the NCS twofold axis. (*c*) The orthorhombic dimer viewed in a random orientation illustrating the approximately 1000 $Å^2$ interface that exists between the two molecules. In each part, the *A* chain is in yellow and the *B* chain is in blue. The A and B domains of each molecule in (*a*) are shown in different shades. NADP and ATR are shown as atom spheres in (*a*) and (*b*).

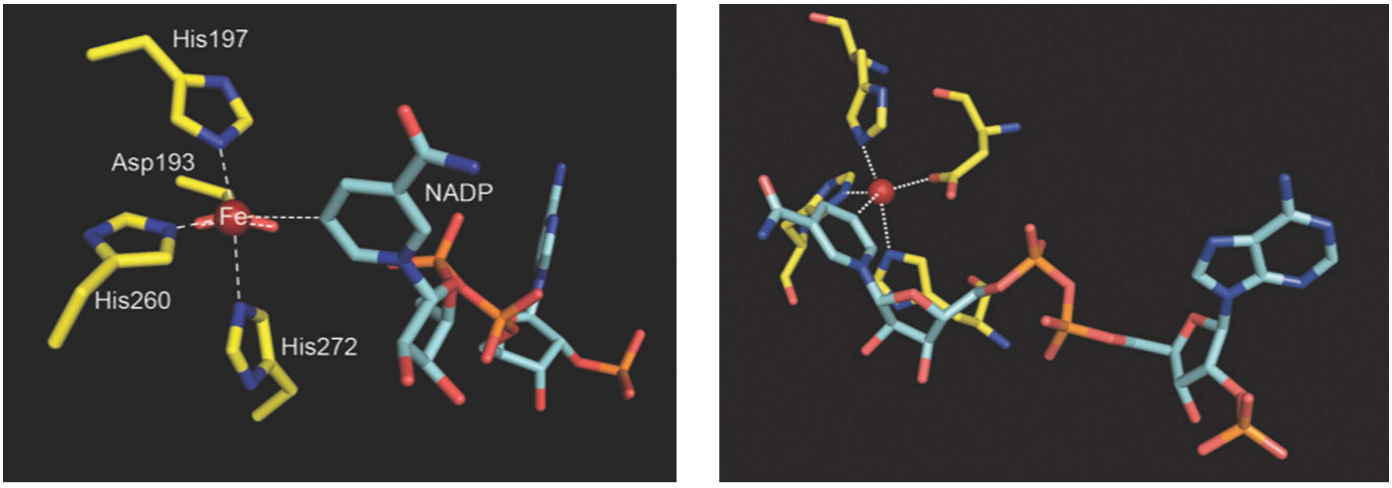

(*a*) (*b*)

Figure 2
Fe-atom binding site. (*a*) shows the Fe atom bound by the protein through a trigonal bipyramidal coordination, with Asp193, His260 and C5N of NADP at the corners of the trigonal plane and His197 and His272 in the axial positions. The NADP is in van der Waals contact with the Fe atom, which is presumably in the ferric state. The view in (*b*) is rotated approximately 90° from that in (*a*). Here it can be seen that the nicotinamide ring is edge-on, with C5N directed towards the iron.

Supplementary Table S1*b*). The exact twofold symmetry in the latter crystals is broken by the binding of coenzyme and an Fe atom by one subunit of a pair (Fig. 1) and the consequent conformational changes (see below) with respect to the other subunit. This same dimer relationship was seen in the *T. maritima* structure (Supplementary Table S1*b*).

Like almost all dehydrogenases (Brändén & Tooze, 1991; Petsko & Ringe, 2004), the enzyme can be divided into two domains: A (amino acids 1–182) and B (amino acids 183–378). The detailed arrangement of helices, sheets and strands in the domains have been described for the *T. maritima* enzyme (Schwarzenbacher *et al.*, 2004), and are virtually the same in the *T. thioreducens* enzyme (Fig. 1). Domain A contains a nucleotide-binding fold (Brändén & Tooze, 1991), which is responsible for binding the coenzyme, while domain B provides all of the ligands for the metal ion. With respect to the *T. maritima* enzyme, there is a seven-residue insertion in a loop between a β-strand and an α-helix in domain A at residues 117–123 and an eight-residue insertion in a loop between two α-helices in domain B at residues 308–315.

The domains have the potential to alter their relative orientation through a tenuous hinge segment (amino acids 181–183). The B domains in the five molecules reported here are very similar regardless of the presence of NADP (the average r.m.s.d. is 0.34 Å), whereas there is a distinct change in the A domains in relation to the B domains between NADP-

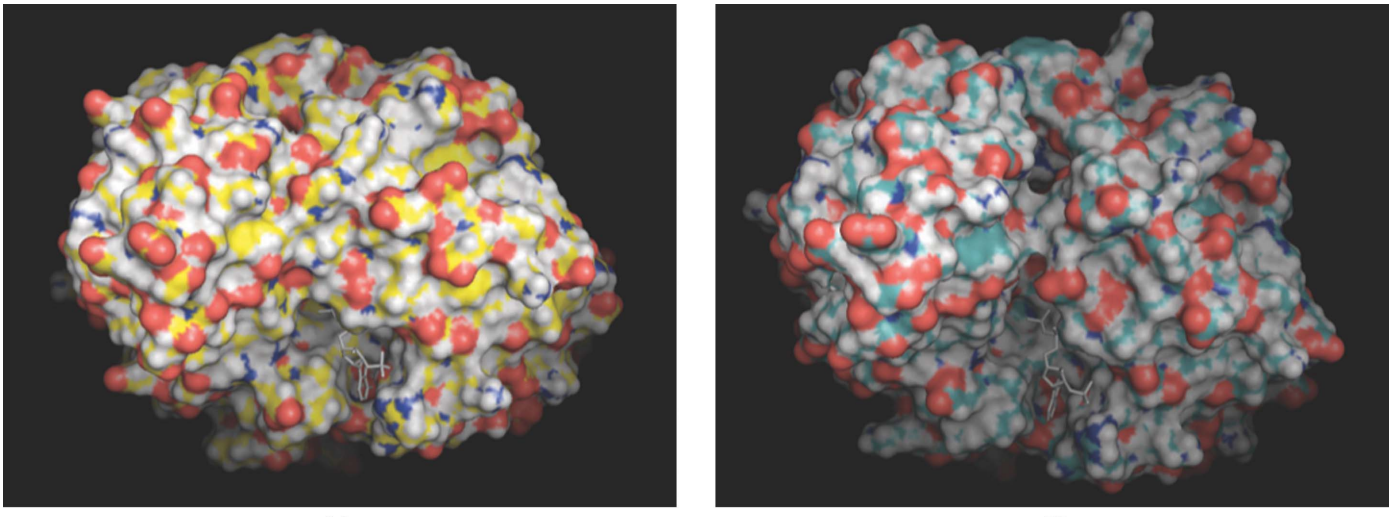

(*a*) (*b*)

Figure 3
Coenzyme binding. Comparison of the surfaces of the *A* and *B* chains of the monoclinic cell viewed perpendicular to the coenzyme tunnel. (*a*) Chain *A* with the adenine end of NADP protruding from the tunnel at the bottom; the surface is closed from the tunnel opening at the bottom to the top of the molecule. (*b*) Chain *B* with ATR protruding from the tunnel at the bottom; the surface is much more open over the tunnel than in (*a*).

bound and unbound molecules (see Supplementary Table S1). Superposition of the C^{α} atoms of the B domains of molecules *A* and *B* in each of the monoclinic and orthorhombic crystals followed by superposition of the C^{α} atoms of the A domains results in a rotation of the A domain with respect to the B domain upon NADP binding in each crystal form (in the range 5.4–8.1°). The nucleotide-binding domain A provides all of the ligands for the NADP (see Supplementary Table S2). The Fe atom is bound to the second domain by the side chains of His197, His260, His272 and Asp193, which occupy four of the five positions of a trigonal bipyramid around the Fe atom (Fig. 2 and Supplementary Table S3).

A noteworthy connection between the two domains involves the C5N atom of the nicotinamide ring of NADP. This ring spans the domains and approaches the Fe atom edge-on such that C5N and its bound H atom are within van der Waals distance of the Fe atom, occupying the fifth position (third equatorial position) of the trigonal bipyramidal arrangement of ligands around the iron (Supplementary Table S3 and Fig. 2). This same disposition of the Fe atom, coenzyme and protein is seen in both the monoclinic and orthorhombic crystal forms and in the *T. maritima* structure (Supplementary Table S3). Both the Fe atom and the coenzyme are absent in molecules *B* of the monoclinic and orthorhombic cells, and in the tetragonal structure, where the protein appears to be in a more open conformation (Fig. 3 and Supplementary S4).

The temperature factor of the Fe atom in the monoclinic crystals is 70 $Å^2$, while the average *B* factor of molecule *A*, to which the iron is bound, is 62 $Å^2$ and that of NADP is 71 $Å^2$. In the orthorhombic crystals, the Fe-atom *B* factor is slightly lower at 65 $Å^2$, but so are the average *B* factors of molecule *A* at 38 $Å^2$ and NADP at 31 $Å^2$. The value of the *B* factor for the Fe atom, which is comparable to those of the protein and NADP, in the former case suggest that the Fe-atom site is likely to be fully occupied, or nearly so; in the latter case, it is considerably less likely to be fully occupied. In the tetragonal case we have modeled 19 phosphate ions, including a 40% occupied phosphate–water structure overlaid on the partially occupied ATR model. By contrast, in the model for the enzyme from *T. maritima* there were 892 waters.

4. Discussion

Superposition of the B domains of protein molecules with bound coenzyme and iron (monoclinic and orthorhombic crystals) with molecules lacking NADP (all three crystal forms) shows that there is consistently a rotation of the A domains by 5° or greater as a consequence of NADP and iron binding (Supplementary Fig. S5). Fig. 5 shows the change that occurs at loops 61–69, 147–165 and 107–123 of the A domain that form one wall of the tunnel. Of these three loops, only loop 147–165 makes direct interactions with NADP through Ser148, Asp150 and Lys159 (see Supplementary Table S2), and all of these interactions involve the nicotinamide-ribosyl moiety of NADP. The interaction of Lys159 with the ribose pulls loop 147–165 down to the NADP and the interactions of this central loop with the adjacent loops pulls them with it. There is a minor restructuring of loop 107–123, but this is some distance from the active site and does not appear to be important to function. The largest displacement of C^{α} atoms in loop 147–165 upon NADP binding occurs for Gly156 (range 6.7–8.4 Å). The key interaction appears to be between Lys159 and the ribosyl moiety. Ala150 and Ser148, which interact with the amide group of the nicotinamide, do not move significantly between the NADP-bound and unbound states. The loop residues are on the opposite side of the nicotinamide ring from the iron and therefore do not significantly influence its immediate environment.

The second significant change is in a turn–helix designated loop 61–84 in Fig. 4. The helix translates along its axis between 2 and 5 Å for the three non-NADP-bound molecules. This turn–helix makes hydrogen-bonding interactions with loop 147–165 and appears to be pulled along by the latter. By inspection, neither of these two changes in conformation, which are apparently triggered by the binding of the Fe atom and NADP, perceptibly alters the binding interactions of the protein with the coenzyme except for Lys159. This is clear from the presence of ATR in the monoclinic and tetragonal structures (see Supplementary Table S2). The movement of the turn–helix causes Glu65 to reach across the coenzyme-binding site to form a hydrogen bond to the peptide N atom of His272, essentially pulling the top over the coenzyme tunnel. Both conformational changes occur near the nicotinamide end of the fully extended NADP and neither would affect interactions with the adenosine moiety or any of the three phosphate groups. The likelihood is that these conformational changes reconfigure the area surrounding the nicotinamide to create an appropriate and specific binding site for the alcohol or aldehyde substrate.

The Fe atom is buried in the interior of the enzyme and the exits are obstructed by the coenzyme. Thus, it appears likely

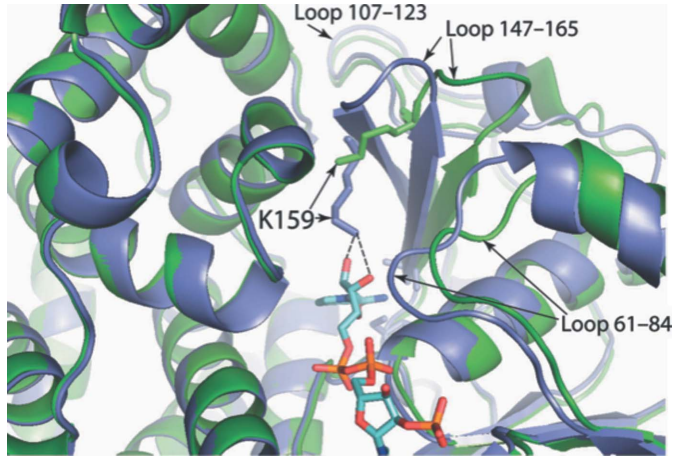

Figure 4
Domain comparison. Domain B of chain *B* (green) of the orthorhombic crystal superposed on domain B of chain *A* (blue) of the same crystal form, illustrating the movement of the three identified loops or segments of domain A upon NADP binding. Lys159 moves down into the NADP-binding cleft to hydrogen-bond to the hydroxyl groups of the ribose ring bound to the nicotinamide ring. When the nicotinamide riboside portion of NADP is absent, the loops are in an open conformation and Lys159 is directed elsewhere, as seen here.

from our observations on all of the crystal forms that the binding of the Fe atom and NADP may be a cooperative process, and that one is bound only in concert with the other. No examples of FeADH have been reported in which either iron or NADP were bound alone. The active site of the enzyme is architecturally noteworthy. As shown by the surface rendering of the molecule in Fig. 5(*a*), there is a broad, completely enclosed tunnel of about 10 Å in diameter at the adenine end that penetrates the protein between the domains and passes all the way through it from one side to the other, tapering down to about 4 Å at the exit at the nicotinamide end. There is approximately 10 Å of empty space (disregarding water) from beyond the nicotinamide ring to the exit of the tunnel (see Supplementary Figs. S6*b*, S6*d* and S7). The iron must diffuse through the tunnel to be bound in the interior. The coenzyme then almost fills the tunnel as it extends across the protein, as shown in Fig. 5(*c*) and Supplementary Fig. S6. The nicotinamide moiety faces the exterior through the distal end of the tunnel (Fig. 5*d*), which must in turn accommodate the substrate. The buried tunnel-like binding site of NADPH suggests that binding and release of the cofactor has to be accompanied by enzyme dynamics. Alternatively, the cofactor might be reduced while still bound to the enzyme.

The protein molecule in the tetragonal crystal form is superimposable, within the error of this structure determination, upon the molecules in the other two crystal forms that lack iron and coenzyme (average r.m.s.d. of 0.63 Å; Supplementary Table S3*a*). However, unlike the other forms, the tetragonal form was grown using a high concentration of ammonium phosphate. A persistent issue in the refinement process was the presence of many phosphate ions associated with the protein, 19 of which were eventually modeled at various occupancies. Initially, phosphates were modeled at every NADP phosphate site in the tunnel until it became obvious that these phosphates were actually part of the 2′-monophosphoadenosine 5′-diphosphate molecule, which

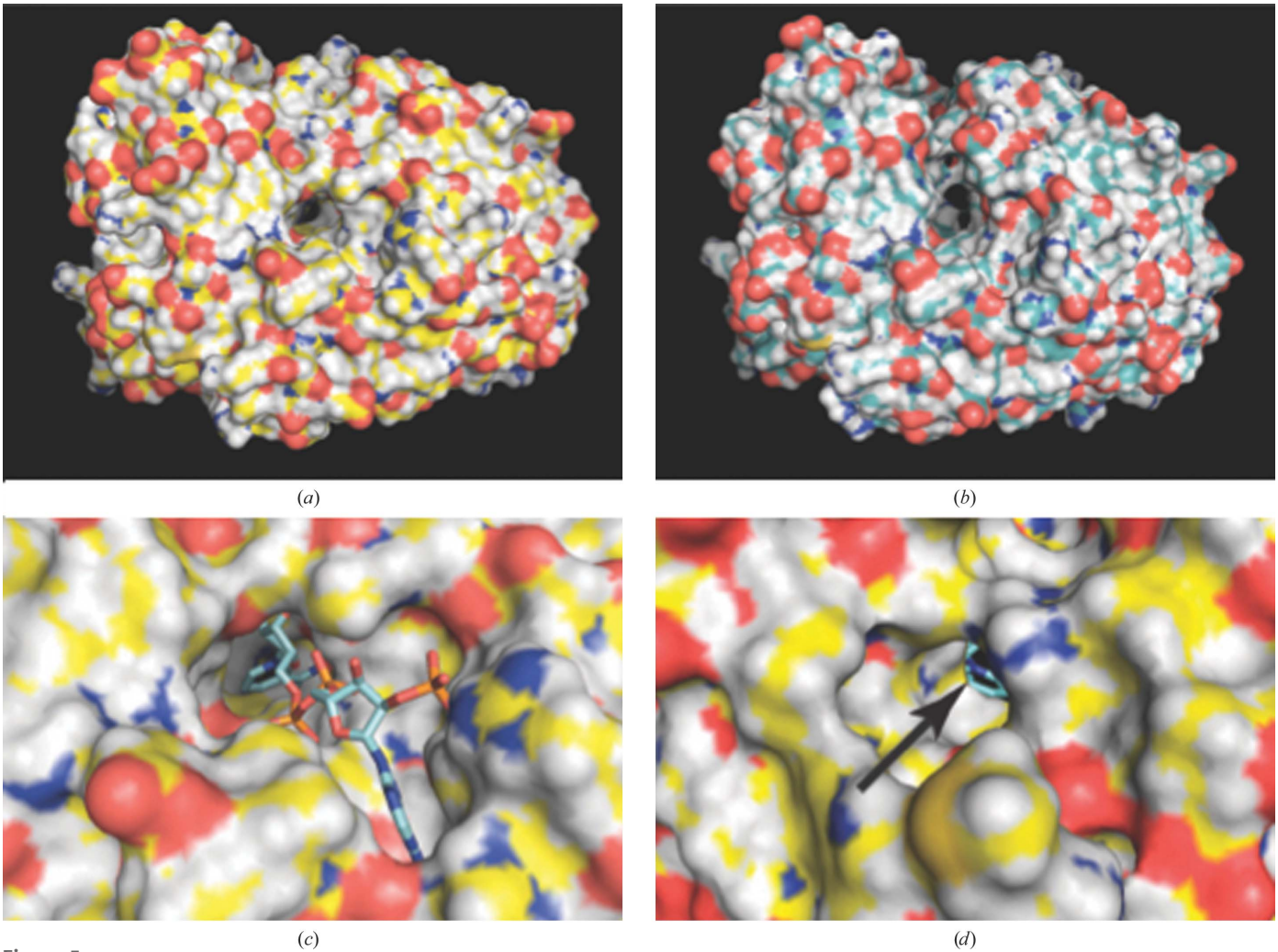

Figure 5
The coenzyme tunnel. (*a*) The FeADH chain *A* molecule from the orthorhombic crystals with the iron and NADP removed. (*b*) The FeADH chain *B* molecule from the same crystal form, which has no iron or coenzyme bound. The unobstructed tunnel that passes all the way through each molecule from one side to the other is evident here, but the top of the tunnel is more open owing to the difference in the relative positions of the A domain with respect to the B domain when NADP and iron are not bound in the tunnel. (*c*) A close-up view of NADP bound in the tunnel of the orthorhombic crystal, showing how the proximal end of the tunnel is completely filled by NADP. In (*d*) the view is into the distal end of the tunnel with coenzyme bound, showing the disposition of the nicotinamide ring (indicated by an arrow) and, presumably, the substrate-binding site.

was ultimately modeled at 60% occupancy. In the final model there is a fully occupied phosphate bound to Asp193, His197, His260 and His264, which is a proxy for the missing Fe atom, and a 40% occupied phosphate overlapping the last phosphate of the ATR diphosphate group but shifted towards the nicotinamide cavity.

X-ray data for the unliganded protein crystal (tetragonal form) were collected at cryogenic temperature rather than at room temperature as for the other crystal forms. No appreciable difference was seen, at least in the backbone trace, between the molecules in the tetragonal form and the unliganded molecules in the other crystal forms. Hence, it does not appear that differences in temperature or ionic strength made any significant conformational difference.

In the course of this analysis, we observed coenzyme binding where no nicotinamide moiety appeared to be present, which we modeled as ATR. There are two plausible explanations. One is that ATR rather than NADP is in fact bound. This implies that the nicotinamide ring was removed from NADP prior to crystallization and was bound in place of NADP. The second possibility is that NADP is bound, but the nicotinamide ring is so disordered that it provides no electron density. We favor the second alternative. Although enzymes exist that remove the nicotinamide moiety from NADP to produce ATR, they are rare, and there is no evidence that they are present in *T. thioreducens*. Any reluctance to accept disorder arises from the restricted space occupied by the nicotinamide when it is observed as NADP. We note, however, that ATR is seen in place of NADP only when iron is absent.

In the absence of iron, additional space around the nicotinamide site is created and this would probably allow the nicotinamide to have the freedom to assume multiple or even random orientations and thus be invisible in electron-density maps. This is likely to be the correct explanation for the ATR. An implication, however, is that the Fe atom and its induced environment are essential for the ordering of the nicotinamide ring and subsequent catalytic activity.

5. Related literature

The following references are cited in the Supporting Information for this article: Brünger *et al.* (1998) and Hammes-Schiffer & Benkovic (2006).

Acknowledgements

The authors wish to thank Professor Joseph Ng of the Chemistry Department at the University of Alabama at Huntsville for the generous gift of the alcohol dehydrogenase protein, which was produced by his company iXpressGenes (Huntsville, Alabama, USA). He is also thanked for providing detailed information regarding the providence of the protein. We also thank Jim Pflugrath for his help in collecting and processing the data obtained for the tetragonal crystal form.

References

Battye, T. G. G., Kontogiannis, L., Johnson, O., Powell, H. R. & Leslie, A. G. W. (2011). *Acta Cryst.* D**67**, 271–281.
Blessing, R. H. (1997). *J. Appl. Cryst.* **30**, 176–177.
Brändén, C.-I. & Tooze, J. (1999). *Introduction to Protein Structure*, 2nd ed. New York: Garland.
Brünger, A. T., Adams, P. D., Clore, G. M., DeLano, W. L., Gros, P., Grosse-Kunstleve, R. W., Jiang, J.-S., Kuszewski, J., Nilges, M., Pannu, N. S., Read, R. J., Rice, L. M., Simonson, T. & Warren, G. L. (1998). *Acta Cryst.* D**54**, 905–921.
Eklund, H. & Brändén, C.-I. (1987). In *Biological Macromolecules and Assemblies*, Vol. 3, edited by F. A. Jurnak & A. McPherson. New York: John Wiley & Sons.
Elleuche, S. & Antranikian, G. (2013). *OA Alcohol*, **1**, 3.
Emsley, P., Lohkamp, B., Scott, W. G. & Cowtan, K. (2010). *Acta Cryst.* D**66**, 486–501.
Evans, P. (2006). *Acta Cryst.* D**62**, 72–82.
Evans, P. R. (2011). *Acta Cryst.* D**67**, 282–292.
Evans, P. R. & Murshudov, G. N. (2013). *Acta Cryst.* D**69**, 1204–1214.
Hammes-Schiffer, S. & Benkovic, S. (2006). *Annu. Rev. Biochem.* **75**, 519–541.
Liu, X., Dong, Y., Zhang, J., Zhang, A., Wang, L. & Feng, L. (2009). *Microbiology*, **155**, 2078–2085.
Ma, K. & Adams, M. W. W. (1999). *J. Bacteriol.* **181**, 1163–1170.
Marsic, D., Hughes, R. C., Byrne-Steele, M. L. & Ng, J. D. (2008). *BMC Biotechnol.* **8**, 44.
McCoy, A. J., Grosse-Kunstleve, R. W., Adams, P. D., Winn, M. D., Storoni, L. C. & Read, R. J. (2007). *J. Appl. Cryst.* **40**, 658–674.
McPherson, A. (1982). *The Preparation and Analysis of Protein Crystals.* New York: John Wiley & Sons.
McPherson, A. (1999). *The Crystallization of Biological Macromolecules.* New York: Cold Spring Harbor LaboratoryPress.
McPherson, A. & Gavira, J. A. (2014). *Acta Cryst.* F**70**, 2–20.
Minor, W., Cymborowski, M., Otwinowski, Z. & Chruszcz, M. (2006). *Acta Cryst.* D**62**, 859–866.
Montella, C., Bellsolell, L., Pérez-Luque, R., Badía, J., Baldoma, L., Coll, M. & Aguilar, J. (2005). *J. Bacteriol.* **187**, 4957–4966.
Moon, J.-H., Lee, H.-J., Park, S.-Y., Song, J.-M., Park, M.-Y., Park, H.-M., Sun, J., Park, J.-H., Kim, B. Y. & Kim, J.-S. (2011). *J. Mol. Biol.* **407**, 413–424.
Murshudov, G. N., Skubák, P., Lebedev, A. A., Pannu, N. S., Steiner, R. A., Nicholls, R. A., Winn, M. D., Long, F. & Vagin, A. A. (2011). *Acta Cryst.* D**67**, 355–367.
Murshudov, G. N., Vagin, A. A. & Dodson, E. J. (1997). *Acta Cryst.* D**53**, 240–255.
Persson, B., Hedlund, J. & Jörnvall, H. (2008). *Cell. Mol. Life Sci.* **65**, 3879–3894.
Petsko, G. A. & Ringe, D. (2004). *Protein Structure and Function.* London: New Science Press.
Pflugrath, J. W. (2004). *Methods*, **34**, 415–423.
Pflugrath, J. W. (2015). *Acta Cryst.* F**71**, 622–642.
Pikuta, E. V., Marsic, D., Itoh, T., Bej, A. K., Tang, J., Whitman, W. B., Ng, J. D., Garriott, O. K. & Hoover, R. B. (2007). *Int. J. Syst. Evol. Microbiol.* **57**, 1612–1618.
Radianingtyas, H. & Wright, P. C. (2003). *FEMS Microbiol. Rev.* **27**, 593–616.
Sambrook, J., Fritsch, E. F. & Maniatis, T. (1989). *Molecular Cloning: A Laboratory Manual.*, 2nd ed. New York: Cold Spring Harbor Laboratory Press.
Schwarzenbacher, R., von Delft, F., Canaves, J. M., Brinen, L. S., Dai, X., Deacon, A. M., Elsliger, M. A., Eshaghi, S., Floyd, R., Godzik, A., Grittini, C., Grzechnik, S. K., Guda, C., Jaroszewski, L., Karlak, C., Klock, H. E., Koesema, E., Kovarik, J. S., Kreusch, A., Kuhn, P., Lesley, S. A., McMullan, D., McPhillips, T. M., Miller, M. A., Miller, M. D., Morse, A., Moy, K., Ouyang, J., Page, R., Robb, A., Rodrigues, K., Selby, T. L., Spraggon, G., Stevens, R. C., van den Bedem, H., Velasquez, J., Vincent, J., Wang, X., West, B., Wolf, G., Hodgson, K. O., Wooley, J. & Wilson, I. A. (2004). *Proteins*, **54**, 174–177.
Walsh, C. (1979). *Enzymatic Reaction Mechanisms*, ch. 10. New York: W. H. Freeman & Co.